Title
Estimating cloud top height and spatial displacement from scan-synchronous GOES images using simplified IR-based stereoscopic analysis

Journal
Journal of Geophysical Research, 105(D12)

ISSN
0148-0227

Authors
Mahani, Shayesteh E
Gao, Xiaogang
Sorooshian, Soroosh
et al.

Publication Date
2000-06-27

DOI
10.1029/2000jd900064

JOURNAL OF GEOPHYSICAL RESEARCH, VOL. 105, NO. D12, PAGES 15,597–15,608, JUNE 27, 2000

Estimating cloud top height and spatial displacement from scan-synchronous GOES images using simplified IR-based stereoscopic analysis

Shayesteh E. Mahani, Xiaogang Gao, Soroosh Sorooshian, and Bisher Imam

Department of Hydrology and Water Resources, University of Arizona, Tucson

Abstract. An efficient method for estimating cloud top heights and correcting cloud image spatial displacements was developed. The method applies stereoscopic analysis to a pair of scan-synchronous infrared cloud images received from two GOES satellites using a piecewise linear approximation of the relationship between height and infrared brightness temperature of top of the cloud element. The algorithm solves for cloud top heights and subsequently calculates the spatial displacements of cloud images. Optimal parameterization of the piecewise linear approximation is achieved using the shuffled complex evolution (SCE) algorithm. Because the proposed method simplifies the stereoscopic analysis, it allows for an easy implementation of stereoscopic technique on desktop computers. When compared to the standard isotherm matching approaches, the proposed method yielded higher correlation between GOES 8 and GOES 9 scan- simultaneous images after the parallax adjustment. The validity of the linear approximation was tested against temperature profiles obtained from the multiple ground sounding measurements from the Tropical Rainfall Measuring Mission/Texas and Florida Underflights (TRMM/TEFLUN) experiments. The results of this comparison demonstrated good fit, particularly within the troposphere, between the optimized relationship and atmospheric sounding measurements. The data produced by this method, including cloud top temperatures and heights, atmospheric temperature profiles for cloudy sky areas, and spatial displacement-adjusted cloud images, can be useful for weather/climate and atmospheric studies. In particular, the displacement-adjusted cloud images can be critical to develop high-resolution satellite rainfall estimates, which are urgently needed by mesoscale atmospheric modeling and studies, severe weather monitoring, and heavy precipitation and flash flood forecasting. Limitations of the proposed method are also identified and discussed.

1. Introduction

Recent advances in understanding atmospheric properties, particularly those pertaining to cloud and precipitation, have, to a large extent, been aided by satellites. Modern geosynchronous weather satellites provide full-scope dynamic views of clouds and precipitation systems at a wide range of spectral bands and at high spatial and temporal resolutions. Many of the recent geosynchronous satellites employ multiple specific channels, such as the CO_2, water vapor, and "infrared window" channels, in the derivation of moisture and temperature profiles of the atmosphere. This technique, widely known as "satellite sounding", is now a standard operational process at the U.S. National Environmental Satellite, Data, and Information Service (NESDIS) as well as at the European Satellite Operation Center (ESOC). In general, cloud height is estimated from satellite soundings using the infrared window (IRW) technique, the CO_2/IRW ratio algorithm, and the H_2O-IRW intercept method [*Nieman et al.*, 1993]. While satellite sounding systems use images from a single satellite and work in the clear-sky conditions, the geographical separation "parallax" of cloud images obtained simultaneously from two satellites can be used to generate similar information including stereoscopic (three-dimensional (3-D)) and/or 4-D (space and time) visualizations of cloud fields. In fact, shortly after launching the first two U.S. geostationary satellites SMS1 and SMS2, scientists at the Goddard Space Flight Center (GSFC) developed an Atmospheric and Oceanographic Information Processing System (AOIPS) [*Bristor and Pitchel*, 1974; *Minzner et al.*, 1976]. The system applies stereoscopic analyses to simultaneous pairs of images from two satellites, and it incorporates manual interactive parallax measurement algorithms, stereoscopic displays, and cloud height computation algorithms. *Hasler* [1981] and *Hasler et al.* [1991] explored the utility of AOPIS in various meteorological studies, including measurements of cloud top height, cloud base height, cloud emission properties, cloud-type classification, and convective cloud dynamics. The ability to extract 3-D views of cloud fields using 2-D imagery also encouraged researchers to use stereoscopic analysis of satellite data in studying various cloud properties. These include tracking the movement of severe thunderstorms *Fujita*, 1982; *Mack et al.*, 1983; *Hasler et al.*, 1991], tropical

Paper number 2000JD900064.
0148-0227/00/2000JD900064$09.00

cyclones [*Rodgers et al.*, 1983], hurricanes [*Hasler and Morris*, 1986], and the analysis of boundary layer cloud waves and cirrus clouds [*Wylie et al.*, 1998]. The advent of massively parallel processing computers allowed for partial automation of stereoscopic analysis (ASA) [*Strong and Ramapriyan*, 1987; *Hasler et al.*, 1991]. Such automation was, in many cases, a prerequisite for effective implementation of satellite stereoscopy as a cloud analysis tool.

Substantial progress has been made since the 1970s in terms of the quality and the spatial and temporal resolutions of geostationary satellite imagery. The new generation of the National Oceanic and Atmospheric Administration's (NOAA) Geostationary Operational Environmental Satellites (GOES) is equipped with separate imaging and sounding systems, finer spectral resolutions, 10-bit image precision, improved calibration, registration, navigation schemes, and highly efficient data transmission and processing systems [*Menzel and Purdom*, 1994]. GOES and similarly advanced geostationary satellites launched by various nations have formed high-resolution weather-monitoring networks covering a large area of the Earth's surface. The value of this

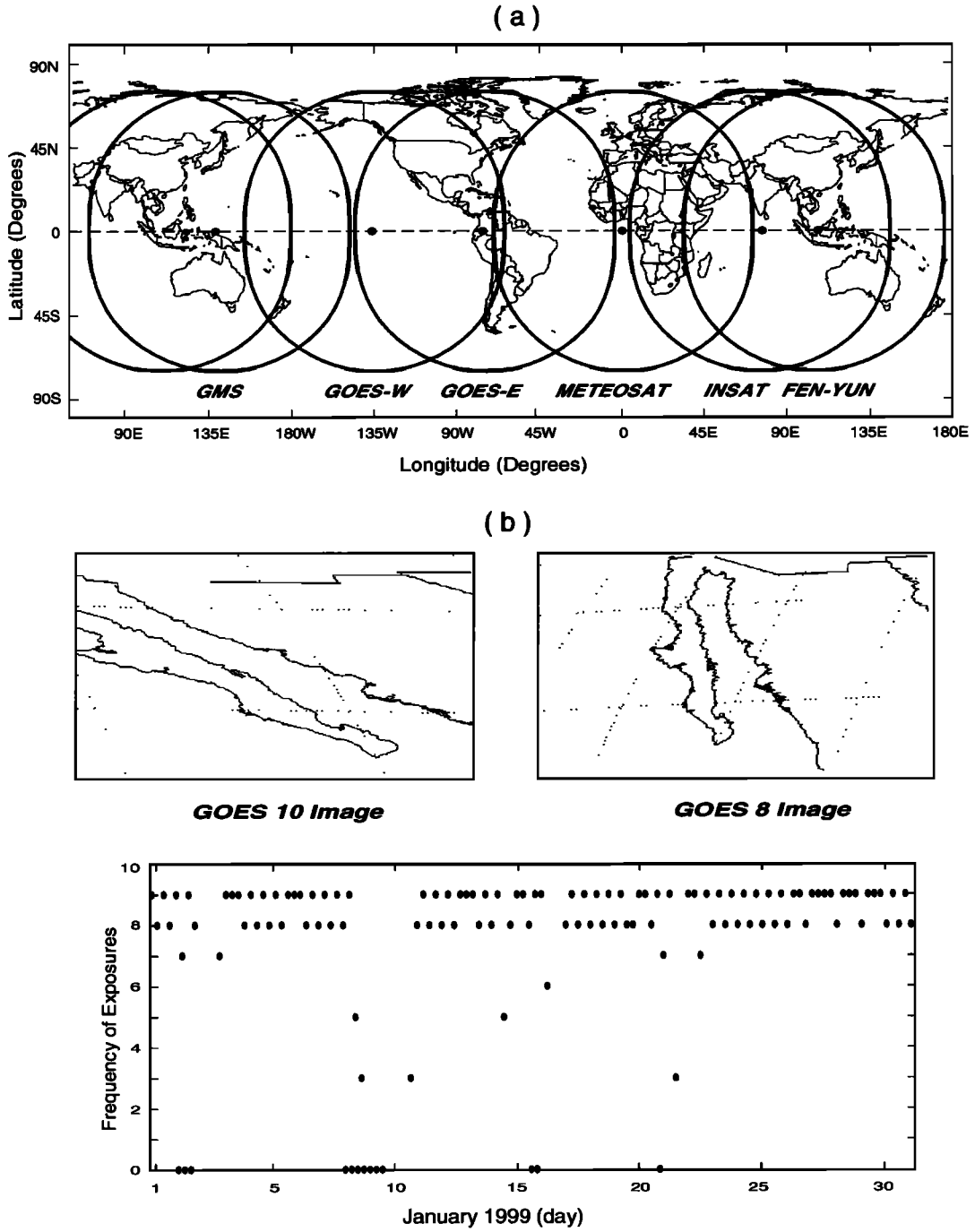

Figure 1. (a) Global coverage of six geostationary satellites. Notice the extent of the regions covered by pairs of satellites as indicated by the intersections of their coverage areas. (b) Six-hour occurrence frequencies of scan-synchronous GOES 8 and GOES 10 IR images over the Baja Peninsula region during January 1999.

network for stereoscopic observations was recognized early on [*Hasler et al.*, 1983]. As shown in Figure 1a, at least six geostationary satellites surround the equator at fixed longitude locations. While each satellite observes a given region, the scan areas of any two adjacent satellites overlap in space and time, leading to multiple scan-synchronous images during any given day. For example, during January 1999, there were 922 pairs of scan-synchronous IR images from GOES 10/west and GOES 8/east over the Baja Peninsula. The 6-hour occurrence frequencies of these pairs, plotted in Figure 1b, show a near-even distribution with an average of seven pairs per 6 hours. Although not all of 922 pairs are likely to include images of clouds, it remains crucial to recognize that the network of geostationary satellites provides an abundant source of data for stereoscopic analyses of cloud properties.

Despite these favorable conditions, wider use of stereoscopic analysis of satellite data has, in general, been impeded by several factors. Satellites, and more importantly, satellite data management systems, are not designed for synchronous operation. Consequently, researchers must search multiple large archive databases to identify scan-synchronous images. In addition, most of the existing stereoscopic techniques use visible bands, which are only available during daytime observations, and thereby provide limited uses to global and large-scale studies. Finally, the significant computational demand and instrumental requirement of the existing stereoscopic techniques render the application of such techniques less than practical and narrowly accessible. Because of these difficulties, recent cloud-relevant research studies programs, such as the International Satellite Cloud Climatology Project (ISCCP) [*Schiffer and Rossow*, 1983; *Rossow and Schiffer*, 1991], the First ISCCP Regional Experiment (FIRE) [*Cox et al.*, 1987], and the Earth Radiation Budget Experiment (ERBE) [*Barkstrom and Smith*, 1986], did not include provisions for satellite stereoscopic observations of clouds in their science plans.

In recent years, the demand for fine-resolution (a few kilometers) cloud and rainfall estimates from satellite observations is rapidly increasing. It is important to mention that this interest is shared by both the researches as well as the operational communities. For example, the hydrologic community has recognized the potential benefit of using remote-sensing information to generate precipitation measurements, particularly over land, for hydrologic applications. These include using the information as a "stand-alone" alert system for heavy precipitation and flash flood warnings and as the atmospheric forcing to drive the distributed hydrologic models for hydrologic predictions. The appeal for this information is especially attractive because traditional in situ observations by rain gauges are relatively sparse, if not completely absent, for many areas of the world. Ground radar observation of precipitation, while available in some developed countries, remains limited, particularly in mountainous regions where radar beams are obstructed. Meanwhile, the community of atmospheric mesoscale modeling also finds that the high-resolution cloud/rainfall data useful for the study of physical and radiative processes of atmosphere and for the 4-D data assimilation (4DDA) procedure to improve the model performances.

In this paper, we attempt to encourage the use of satellite stereoscopic cloud analysis by wider sections of the weather-climate and hydrologic communities. To do so, we introduce a simpler stereoscopic technique, which reduces the computational and hardware requirements of stereoscopic analysis techniques (SAT) and extends their applicability into nighttime by using infrared instead of visible images. Of course, using IR data lowers the spatial resolution of our analysis, but the increased temporal coverage compensates for the lower spatial resolution. The theoretical and algorithmic developments of the method are presented in section 2. In section 3 the results of the proposed method are tested by comparing them with those obtained using the isotherm matching technique and with height-temperature profiles obtained from multiple-sounding measurements. We further evaluate the method by quantifying the improvement in the correlation of scan-synchronous image pairs before and after spatial displacement correction. Finally, in section 4 we provide a summary of the work and point out some of the limitations of the proposed method.

2. Methodology

2.1. Cloud Image Displacement

Herein, a cloud element (A) is defined as a portion of the cloud representing an area of uniform top height. The image of a cloud element is called a pixel. Figure 2 is a schematic illustration of the relationship between the actual position (B) and the apparent (pixel) position (C) of a cloud element (A). The satellite view angle (θ) and the height of the cloud element (h) cause a spatial displacement (r) (from B to C) on the cloud pixel. In general, the displacement vector (r) is a function of the satellite view angle (θ) and the cloud top height (h). Because the altitude of the satellite is substantially higher than that of the cloud, the satellite view angle (θ) depends mainly on the angular distance (α) between the satellite and the cloud element and on the satellite height (H) as well. Therefore, the relationship can be written as

$$r = f(h, \alpha, H). \tag{1}$$

For a single cloud pixel, using the spherical geometry, the angular displacement (γ) (between B and C) is described by

$$R[(H+R)\cos(\alpha)-(R+h)]\sin(\gamma)+R[(H+R)\sin(\alpha)]\cos(\gamma) = (H+R)(R+h)\sin(\alpha) \tag{2}$$

where

γ angular displacement of the cloud pixel;
R local radius of the Earth;
H height of the satellite above Earth;
α angular distance between satellite and cloud element A;
h cloud top height from Earth's surface.

For GOES 8 and GOES 9, $\gamma < 2°$ (e.g., if $\alpha = 75°$ and $h = 15$ km, $\gamma \cong 1.3°$), and its longitudinal γ_λ and latitudinal γ_φ components can be approximated by

$$\gamma_\lambda \cong [h(H+R)\sin(|\lambda_s-\lambda_p|)]/\{R[(H+R)\cos(|\lambda_s-\lambda_p|)-(R+h)]\} \tag{3a}$$

$$\gamma_\varphi \cong [h(H+R)\sin(|\varphi_s-\varphi_p|)]/\{R[(H+R)\cos(|\varphi_s-\varphi_p|)-(R+h)]\} \tag{3b}$$

where λ_s, φ_s are longitude-latitude coordinates of the satellite, and λ_p, φ_p are longitude-latitude coordinates of the

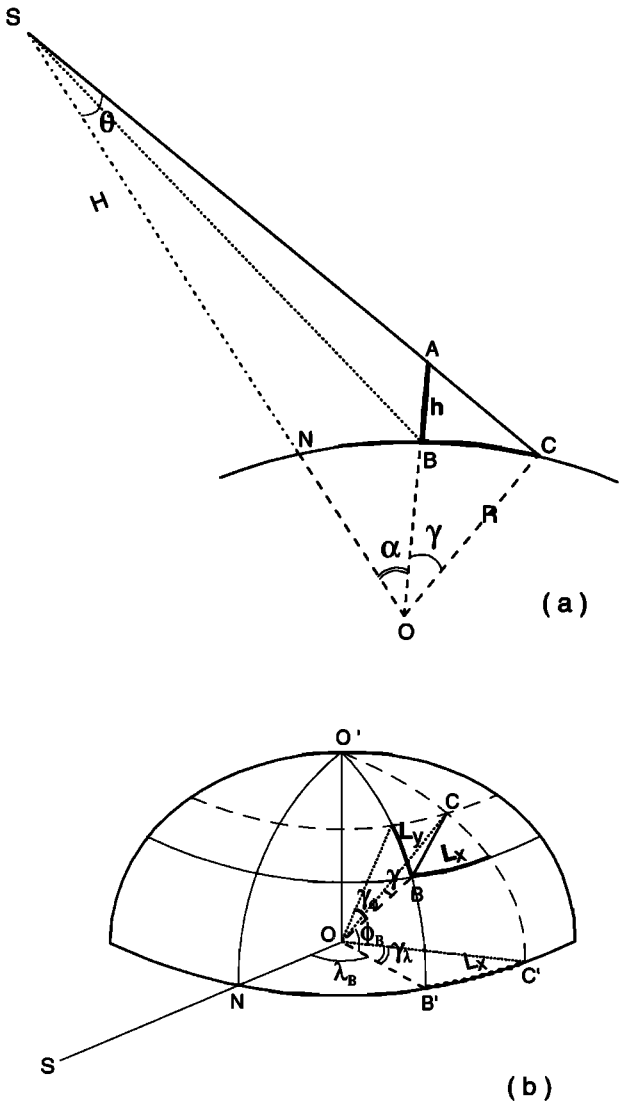

Figure 2. Geometric representation of the spatial displacement calculation: (a) the relationship between angular displacement (γ), cloud top height (h), and satellite view angle (θ); (b) latitudinal and longitudinal components of the spatial displacement for a geostationary satellite image.

cloud element. The linear longitudinal (dL_x) and latitudinal (dL_y) distances of displacements in the case of using geostationary satellite imageries are

$$dL_x = R\,\gamma_\lambda \cos(\varphi_s - \varphi_p) \qquad dL_y = R\,\gamma_\varphi . \tag{4}$$

The variability of the latitudinal displacement for geostationary satellites is shown in Figure 3 as a function of α and h. As expected, the image (pixel) displacement of a cloud element becomes substantial with increases of the angular distance (between the satellite and the cloud element) and cloud top height. For example, when GOES 8 (75°W) views a 10-km-high cloud element over Los Angeles (120°, 30°N), the pixel of this element will shift about 13 km toward the west and 7 km toward the north. In both visible (1-km raw resolution) and IR (4-km raw resolution) observations the apparent location of this cloud element will be several pixels away from its actual geophysical location.

Notice that the cloud image displacements represented in (3) and (4) cannot be solved if the cloud top height is unknown. Because of the difficulty associated with determining cloud top height, current satellite image processing does not account for cloud image displacement errors. Therefore users of high-resolution cloud images should concern themselves with the effect of displacement error for their products, such as the NOAA/NESDIS Satellite Analyses Branch team, which uses manually adjusted parallax correction for the operational satellite rainfall estimate (4 km x 4 km resolution). Our proposed method is an automatic stereoscopic technique.

2.2. Stereoscopic Technique to Estimate Cloud Top Height and Image Displacement

When two satellites simultaneously view a cloud element from different directions, the apparent coordinates of the pixels representing the same cloud element will shift in different directions. This geographical separation of the two corresponding pixels is known as the parallax. The parallax is a measure of the difference between the two displacement vectors (i.e., $|r_1 - r_2|$). In most applications the parallax component that is parallel to the direction between the two satellites is called the x parallax, and the component in the perpendicular direction is called the y parallax. Because the geostationary satellites are located on the equator plane, the latitudinal components of the relief displacements of the pixels representing the same cloud element are the same in magnitude and direction. Therefore the latitudinal (y) parallax does not translate into a visible error. This is demonstrated in Figure 4, which shows the overlapping of brightness temperature contours created from simultaneous GOES 8/east (solid lines) and GOES 9/west (dashed lines) IR images over the Baja Peninsula. By examining the contours, two distinct features emerge. First, it is easy to see that there are x parallaxes between the contours. Second, a closer visual examination reveals that the two contours representing lower brightness temperature (T_b = 210°K) are farther from each other than those representing higher brightness temperature (T_b = 250°K). Therefore, measuring the mean parallax from a pair of T_b isotherms, which represent a group of cloud elements at the same height, will provide the means to resolve for h. Theoretically, this can be achieved by solving a system of equations that consists of one equation (1) for each satellite using the measured values of parallax ($|r_1 - r_2|$). Now the basic procedure of the standard isotherm matching approach can be described: (1) measure the mean parallax ($r_1 - r_2$) for an isotherm pair at a fixed T_b; (2) use ($r_1 - r_2$) and the appropriate ones of equations (1)-(4) to inversely resolve the cloud top height h; (3) substitute h into equation (4) to calculate the displacement, $dL_{x,y}$ and to make displacement correction for all the T_b pixels using $dL_{x,y}$; and (5) change to another isotherm pair with a different T_b and repeating steps 1-4.

The isotherm matching procedure sometimes has difficulty in obtaining good correction. In Figure 4, notice that while the shapes of T_b isotherm pairs are generally similar, they display dissimilarities. Such dissimilarities produce uncertainties in identifying corresponding pixel pairs in the two images and therefore in measuring the parallax. Several factors contribute to the dissimilarity: (1) the difference in sensor bias between the two satellites (i.e., a cloud element is sensed from two satellites and obtained different T_b values); (2) the presence of pixels demonstrating the side of a cloud viewable by one

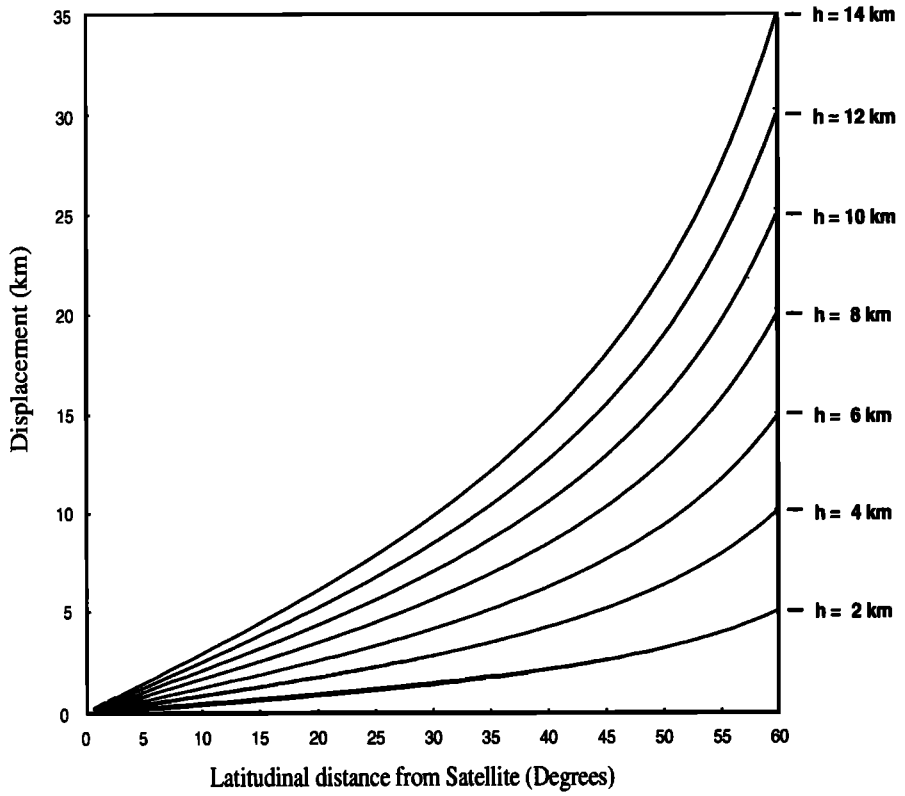

Figure 3. Latitudinal component of pixel displacement as a function of the angular distance between the satellite and the pixel (α) and the cloud top height (h) for a geostationary satellite image.

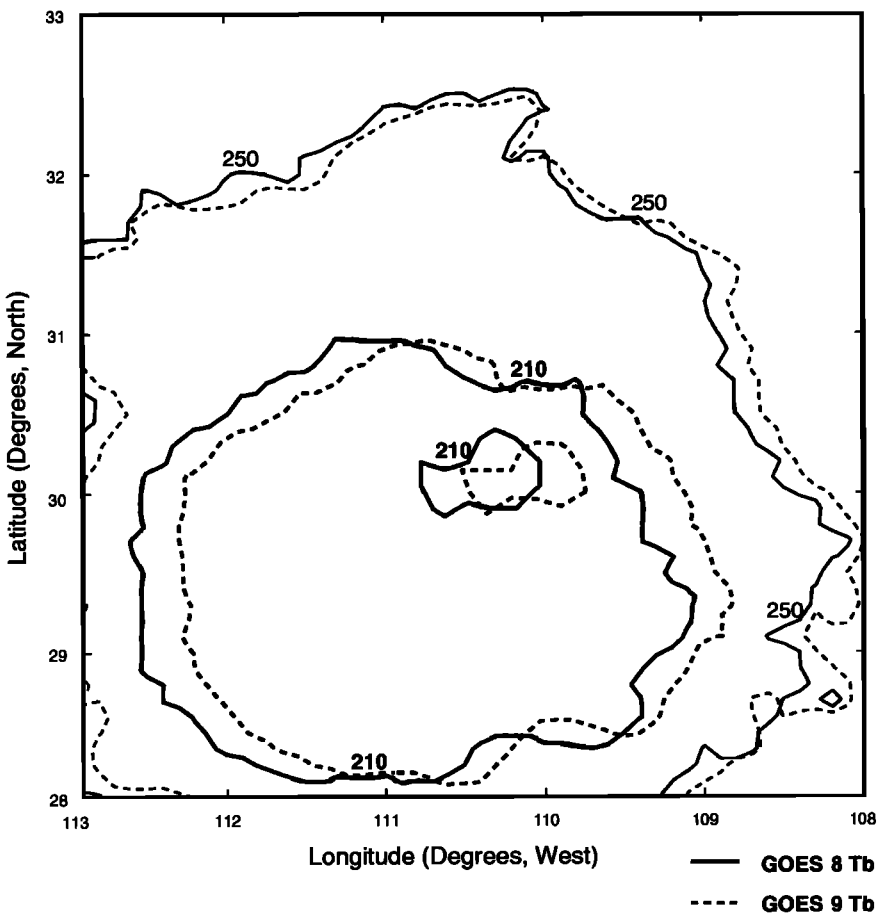

Figure 4. Brightness temperature contours from simultaneous GOES 8 (solid lines) and GOES 9 (dashed lines) IR images over the Baja Peninsula on July 12, 1998, at 0845 UT. The contours represent 210°K and 250°K. Notice that the larger parallax is associated with colder brightness temperature.

satellite but not the other; and (3) the fact that scan-synchronous images are not exactly scan-simultaneous, and the shapes of the isotherms change due to the movement and deformation of the clouds within the short scanning interval.

2.3. Proposed Method

The basic idea of the proposed method is to simplify the image-processing requirements so that it can be automated. If the relationship between the cloud top brightness temperature (T_b) and the cloud top height (h) is known, then the T_b value of a given cloud pixel, which represents its long-wave emission, can be directly used to calculate h as well as the displacements ($dL_{x,y}$). A key issue is then how to accurately identify the T_b-h relationship for different cloud fields. We argue that when cloud temperature reaches equilibrium with the ambient temperature, the T_b-h relationship approaches a linear approximation similar to the commonly used approximation of the relationship between the atmospheric temperature and height (i.e., the lapse rate of atmospheric temperature). In this paper, we propose a piecewise linear approximation to describe the T_b-h relationship:

$$\begin{aligned} h_1 &= h_0 + l_1\,(280 - T_b) && T_1 < T_b \le 280^\circ\mathrm{K} \\ h_2 &= h_1 + l_2\,(T_1 - T_b) && T_2 < T_b \le T_1 \\ h_3 &= h_2 + l_3\,(T_2 - T_b) && T_b \le T_2 . \end{aligned} \tag{5}$$

The parameter h_0 is the height (km) for pixels at T_b = 280°K. In general, h_0 is bounded by the range $h_0 \in [0, 5$ km]. The parameters T_1 and T_2 are temperature thresholds dividing the domain $T_b \le 280$°K into three ranges with $T_1 \in$ [225°K, 265°K] and $T_2 \in$ [215°K, 245°K]. The parameter l_1, l_2, and l_3 describe the slopes (km/°K) of h versus T_b within the three ranges with $l_1 \in [0.08, 0.2]$, $l_2 \in [0.1, 0.2]$, and $l_3 \in [0.125, 0.25]$.

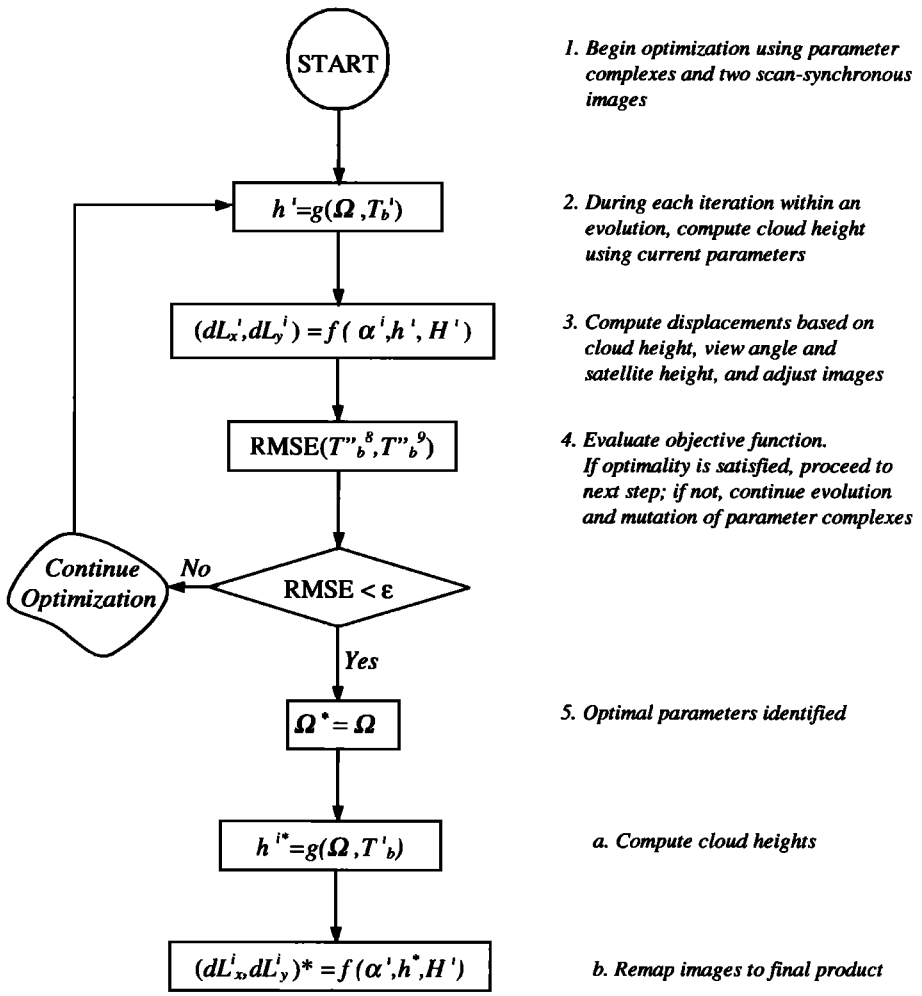

i: Satellite index,
h: Cloud top height,
Ω: Parameter vector (h_0, T_1, T_2, l_1, l_2, l_3),
T_b': Brightness temperature,
dL'_x: Pixel displacements in x direction,
dL'_y: Pixel displacements in y direction,
": Indicates temporary value during optimization,
*: Values correspond to optimal parameter vector.

Figure 5. A flowchart of the optimization procedures for identifying the best parameters of the piecewise linear T_b-height relationship for image adjustment process.

To identify the "best" parameter values (h_0, T_1, T_2, l_1, l_2, l_3) of the linearized T_b-h relationship for a pair of scan-synchronous image matrices, we first introduce an objective function. In this paper, the objective is to minimize the image root-mean-square-error (RMSE) between the brightness temperatures of geographically colocated pixels in the two image matrices. RMSE is calculated as

$$\text{RMSE}(h_0, T_1, T_2, l_1, l_2, l_3) = \left\{\sqrt{\frac{1}{N}\sum_{i,j}[T_b^1(i,j) - T_b^2(i,j)]^2}\right\} \quad (6)$$

where the superscripts 1 and 2 represent the images of satellites 1 and 2, respectively, (i, j) are the pixel coordinates within the image matrices, $T_b(i,j)$ are the brightness temperatures for the pixels located at (i,j), and N is the number of the pixels in the matrix. Second, starting from a group of parameter sets (values of h_0, T_1, T_2, l_1, l_2, l_3 in their ranges) for the piecewise linear T_b-h relationship, the program scans the pixels, one by one, in the image matrices, calculating h and $dL_{x,y}$ according to each "guessed" T_b-h relationship and making pixel position corrections and calculating the RMSE values. Third, an optimization algorithm is called to change the parameter values in the "right" directions and repeating the above processing until the RMSE is minimized. Therefore, when the optimal parameter values are found, the two image matrices are best matched. The processing flowchart of the method is illustrated in Figure 5.

The shuffled complex evolution (SCE-UA) algorithm [*Sorooshian et al.*, 1993] developed in our research group several years ago provided the automatic optimization scheme in our method. The SCE-UA algorithm has been used in several applications, and when compared with other optimization algorithms, it is reported to have superior global optimization efficiency as well as ease of implementation [*Duan et al.*, 1994; *Kuczera*, 1997; *Thyer et al.*, 1999]. For detailed information and the available program of SCE-UA, please see *Sorooshian and Gupta* [1995].

3. Results

3.1. Comparison With Isotherm Parallax Calculation Technique

To test the validity of the proposed linear approximation, independent estimates of cloud top height estimates were obtained using the isotherm matching computation. A pair of simultaneous GOES 8 and GOES 9 images covering a 3.5° x 3.5° area in the Baja Peninsula region (112°W to 108.5°W and 28.5°N to 32°N) at 1130 UT, August 15, 1998, and a pixel size of 0.065° x 0.065° were used. Mimicking the ASA technique to the greatest possible extent, 1°K interval isotherms were generated for each image. The average displacement for each isotherm was calculated using a lag-correlation procedure, which identifies the isotherm displacement by maximizing the correlation between the two images. The same pair of images was used to calculate cloud top height-temperature relationship derived from the best-fit linear approximation. The results of the two processes are compared in Figure 6a, which demonstrates the ability of the piecewise linear approximation to adequately describe the T_b-h relationship. In Figure 6a, the circles are the result of applying the lag-correlation technique to estimate spatial displacement, and l_1, l_2, and l_3 are the slopes of the individual pieces of the line.

The individual pixel T_b values of the two images are plotted against each other for the original images in Figure 6b and after displacement removal in Figure 6c. In comparison to Figure 6b the significantly narrower scattering seen in Figure 6c indicates the improved resemblance between GOES 8 and GOES 9 images as a result of the adjustment. While providing similar accuracy to the isotherm matching approach, the method presented here is more efficient because only six parameters for each pair of images need to be optimized. In contrast to the gradual change in T_b and the pixel-to-pixel matching of isotherms, the SCE-UA optimization of equation (6) is a more simplified alternative.

3.2. Comparison With Atmospheric Soundings

The accuracy of the T_b-h relationship can be assessed with respect to its resemblance to atmospheric sounding of temperature profiles, particularly those made to validate satellite observations. NASA's Tropical Rainfall Measuring Mission (TRMM) validation study included sounding observations of the atmospheric temperature profiles through the Texas and Florida Underflights (TEFLUN) experiments. TEFLUN consisted of a field campaign to collect and archive airborne and ground measurements of the atmospheric and surface variables to coincide with the TRMM satellite data. TEFLUN-A, the first of the TEFLUN experiments, took place between April 1 and May 15, 1998, in eastern Texas (99°W-93°W and 26°N-32°N). TEFLUN-B took place between August 5 and September 28, 1998, in eastern Florida (84°W-79°W and 24°N-31°N). In Figures 7a and 7b, temperature-height profiles of four sounding sites are compared with the optimal linear T_b-h relationships obtained from coincident GOES 8 and GOES 9 images over the TEFLUN-A and TEFLUN-B regions, respectively. Figures 7a and 7b indicate that within the range [220°K-280°K], the RMSE value between the T_b-h relationship and the sounding profiles is ~0.4 km over Texas and ~0.3 km over Florida. The RMSE value in Texas is less than the variance of the sounding data (~0.8 km). Over Florida, however, the derived linear T_b-h relationship underestimates the cloud top heights by ~0.3 km. In general, the linear T_b-h relationship matches well with the sounding data in the troposphere, except for the two boundary ends of the range. The largest deviation between the relationship and the atmospheric profiles occurred below 220°K in Texas and below 200°K in Florida. There are several possible reasons for these deviations. With respect to low temperature (T_b < 220-200°K), clouds experience complex, nonequilibrium thermodynamic processes within the troposphere-stratosphere transition. The complexities of these processes cannot be described easily by linear approximations. On the other hand, for higher temperature ranges (T_b > 280°K) the close proximity of the ground causes large interference from Earth's surface emissions. In both cases, however, one must address the fundamental difference between the "point" profiles observed using atmospheric sounding and the "area average" profiles derived from stereoscopic analysis. The latter uses T_b, which represents an average pixel value, thereby smoothing the differences between the cloud's long-wave emissions and the ambient temperature within the pixel. Further smoothing occurs during

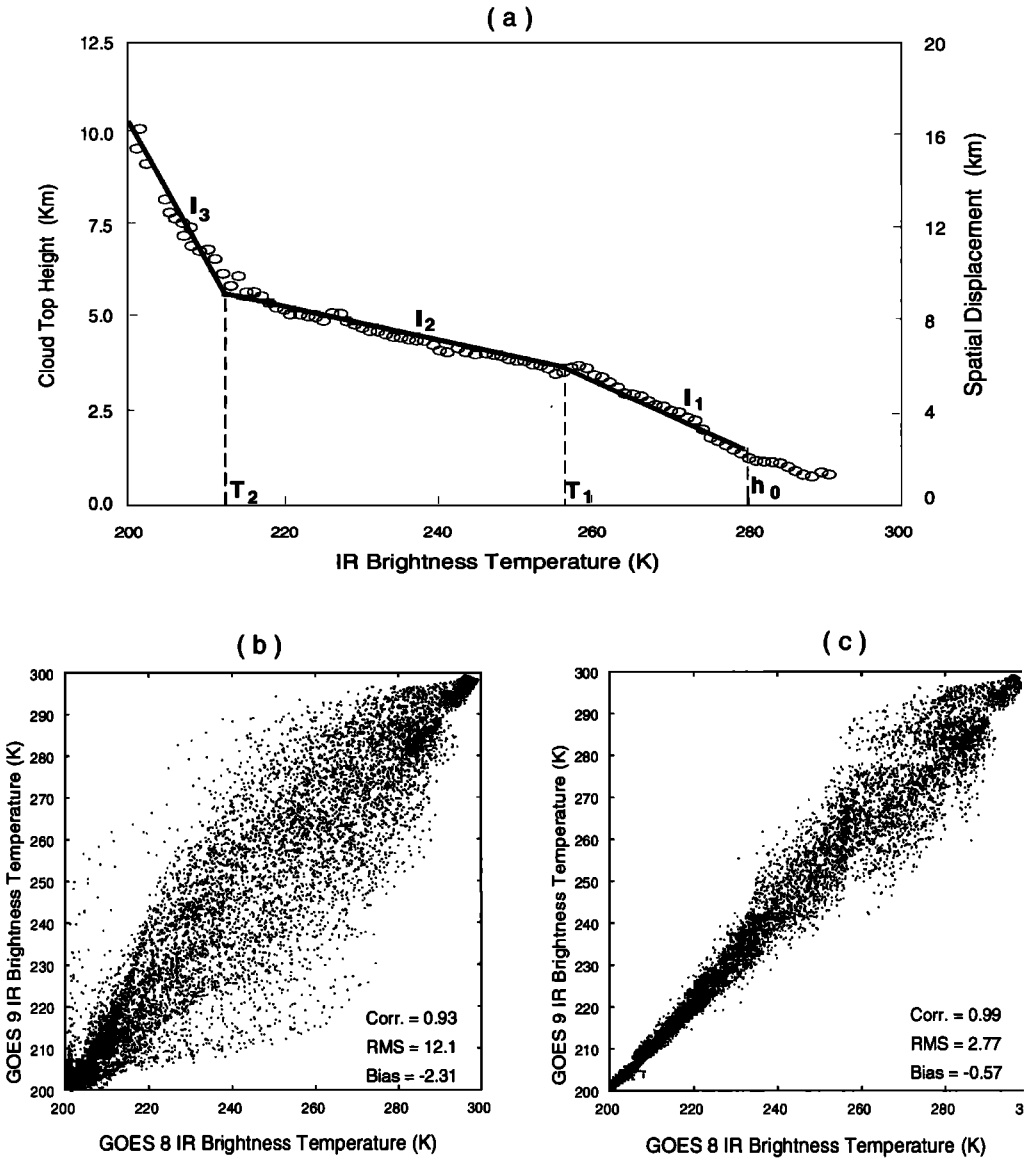

Figure 6. Validity of spatial displacement adjustment and displacement estimating approaches: (a) comparison between T_b-h relationship profiles obtained from the lag-correlation method (circles) and piecewise linear technique; (b) comparison of individual pixel T_b values of the two original GOES images; and (c) comparison of individual pixel T_b values of the two GOES images after removing the spatial displacements.

the identification of the optimal parameters as the objective function takes into account all the pixels within the image matrix.

3.3. Adjustment of Spatial Displacement

To evaluate the potential for improving the quality of IR data using the method described above, 16 scan-simultaneous images from GOES 8 and GOES 9 over four different sites were selected. The location, extent, and timing of the 16 pairs are listed in Table 1. For each pair, SCE-UA was applied to estimate the six parameters of the T_b-h relationship, which was then applied to calculate and remove pixel displacement from both images.

The correlation coefficients and RMSE are plotted in Figures 8a and 8b, respectively. By plotting the two goodness-of-fit values before and after adjustment against each other, a region of improvement is identified as the region above the 1:1 line when an increased value of the goodness of fit is desired and below the 1:1 line when a decrease is preferred. Notwithstanding the initially high correlation between scan-synchronous images of the same area, the correlation coefficients were improved due to adjustment. Similarly, RMSE values show marked improvements. The piecewise linear T_b-h profiles corresponding to the 16 images are plotted in Figure 8c for the Texas and Tucson sites and in Figure 8d for the Baja Peninsula and the Colorado sites. The cross-site and temporal variability of the profiles indicates that the method captured the unique conditions prevalent during each scan.

The image differences between two GOES images before and after adjustment are shown in Plates 1a and 1b, respectively. The images represent pair 9 from Table 1. Noticeable improvement in the resemblance between GOES 8 and GOES 9 due to adjustment can be seen in Plate 1b. The

Table 1. Location, Geographical Extent, and Scan Times of the 16 Pairs of Images Studied Over Four Different Geographic Locations

Location	Extent			Pair No.	Date	Time, UT
	Longitude, °W	Latitude, °N	Size, Pixels			
Texas	99.00	28.00	120x120	1	April 18,1998	0015
	to 93.00	to 32.00		2	April 18,1998	1345
				3	April 18,1998	1602
				4	April 18,1998	1815
Tucson	111.00	27.00	65x65	5	July 12,1998	0445
	to 107.75	to 30.25		6	July 13,1998	0115
				7	July 14,1998	0045
				8	July 15,1998	0145
Colorado	109.00	36.00	140x140	9	Jan. 05,1999	1615
	to 102.00	to 43.25		10	Jan. 05,1999	1345
				11	Jan. 05,1999	0545
				12	Jan. 05,1999	0845
Baja Peninsula	113.00	27.75	100x100	13	July 12,1998	0245
	to 108.00	to 32.75		14	July 12,1998	0415
				15	July 12,1998	0545
				16	July 12,1998	0815

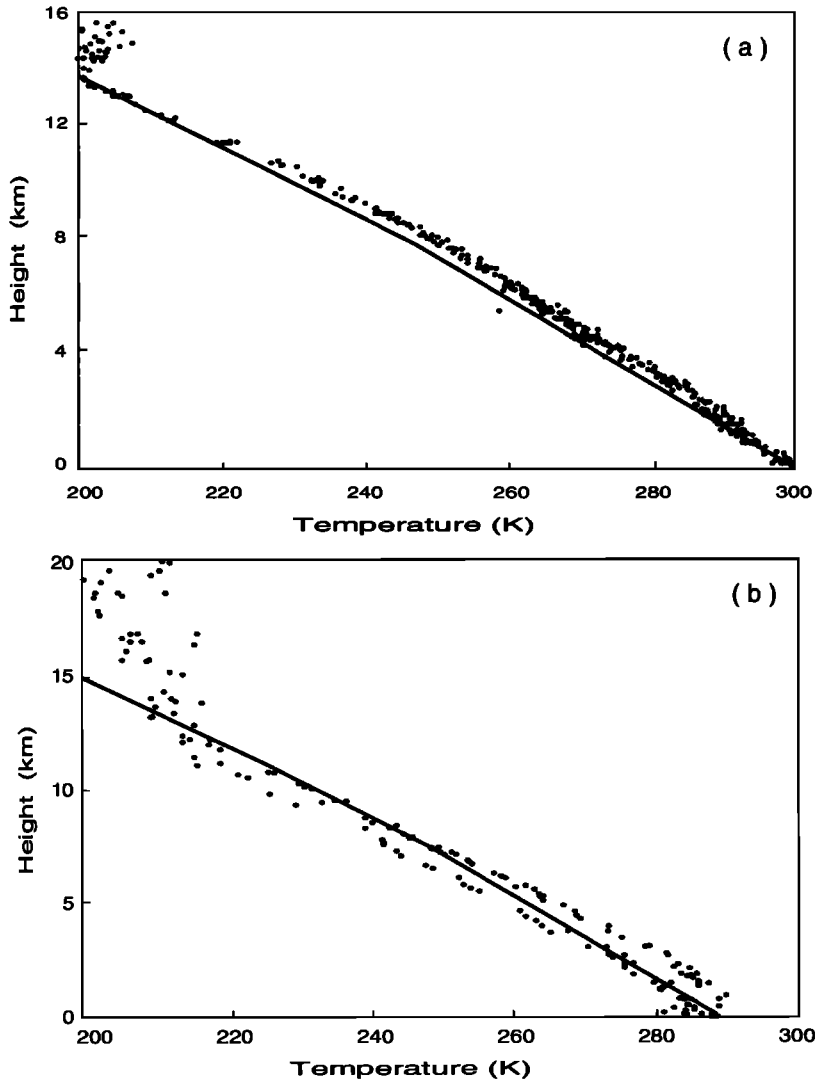

Figure 7. Comparison between the optimal linear T_b-h relationship and atmospheric sounding of temperature-height profile: (a) Florida region (TEFLUN-B) on September 28, 1998, at time 0000UT, and (b) Texas region (TEFLUN-A) on April 18, 1998, at 1200UT noon.

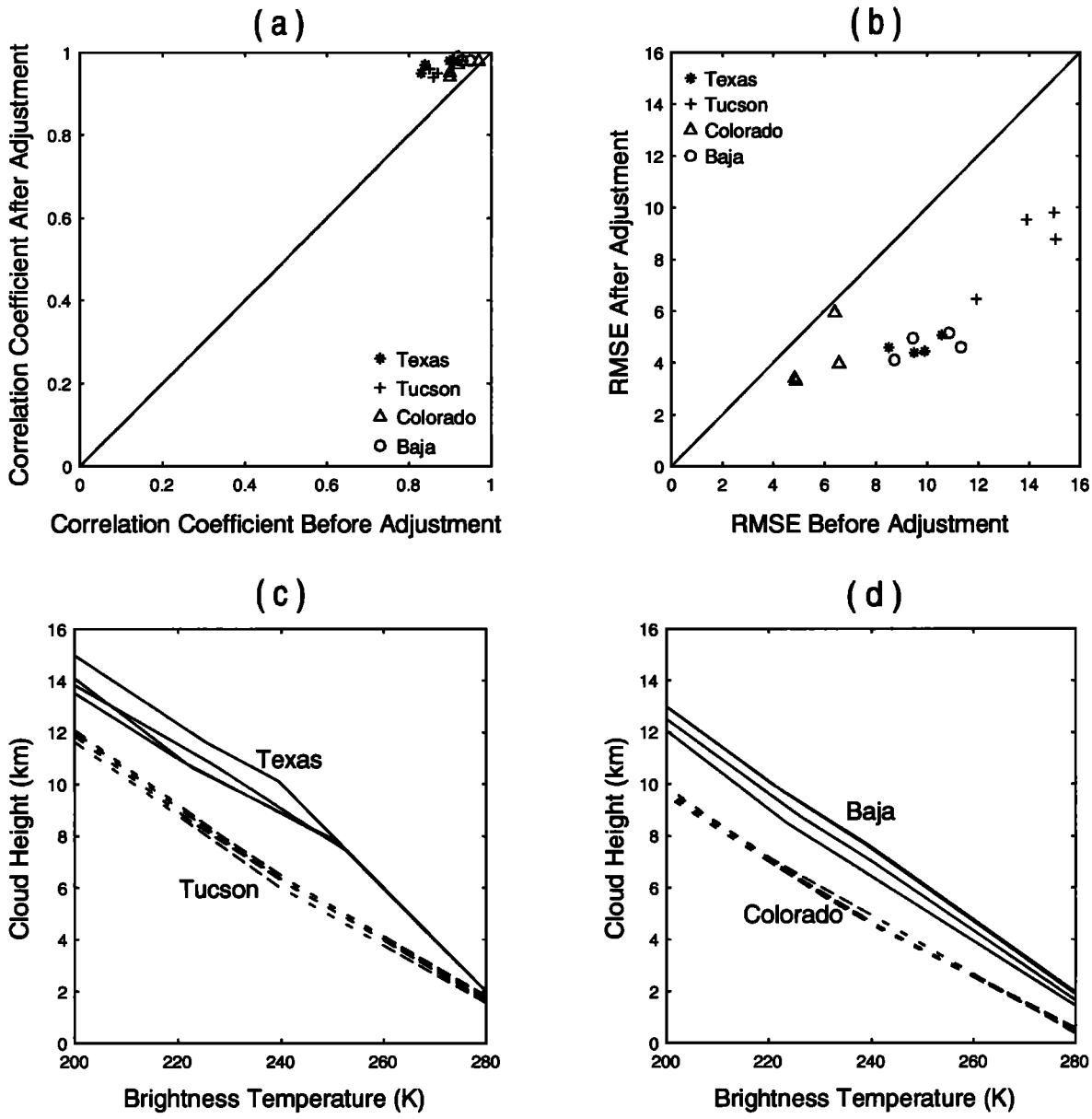

Figure 8. Results of applying the proposed method to 16 simultaneous IR GOES 8 and GOES 9 images: (a) comparison of correlation coefficients before and after adjustment; (b) comparison of RMSE before and after adjustment; (c) the optimal piecewise-linear T_b -h profiles for the Texas and Tucson sites; and (d) the optimal piecewise-linear T_b -h profiles for the Baja Peninsula and the Colorado sites.

corresponding cloud top height field over the region is shown in Plate 1c, which represents the average of the cloud top height profiles obtained from the two GOES images.

4. Summary and Conclusions

It is important to address the geographical displacement associated with cloud top height on the satellite cloud images particularly when these images are used at spatial resolutions lower than the size of the possible displacements. Because these displacements vary with the satellite view angle and cloud top heights, they represent errors that are difficult to remove without additional cloud top height information. A survey of currently operational geostationary satellites indicates that these satellites form a network provide an abundance of extensive and frequent scan-synchronous images over land as well as over the oceans. These scan-synchronous images are sufficient to retrieve cloud top height information and consequently to correct the displacement errors stereoscopically.

A stereoscopic method using the pairs of scan-synchronous satellite infrared images is proposed. In comparison to other stereoscopic techniques the proposed method eliminates the need for parallax measuring and therefore requires no manual correction and pixel-to-pixel matching. This is achieved through the following components: (1) simplified equations that describe the relationship between spatial displacement, cloud top height, and satellite view angle, (2) a piecewise linear approximation of the T_b -h relationship, and (3) a powerful and efficient optimization algorithm (SCE-UA) to identify the parameters of piecewise linear approximation.

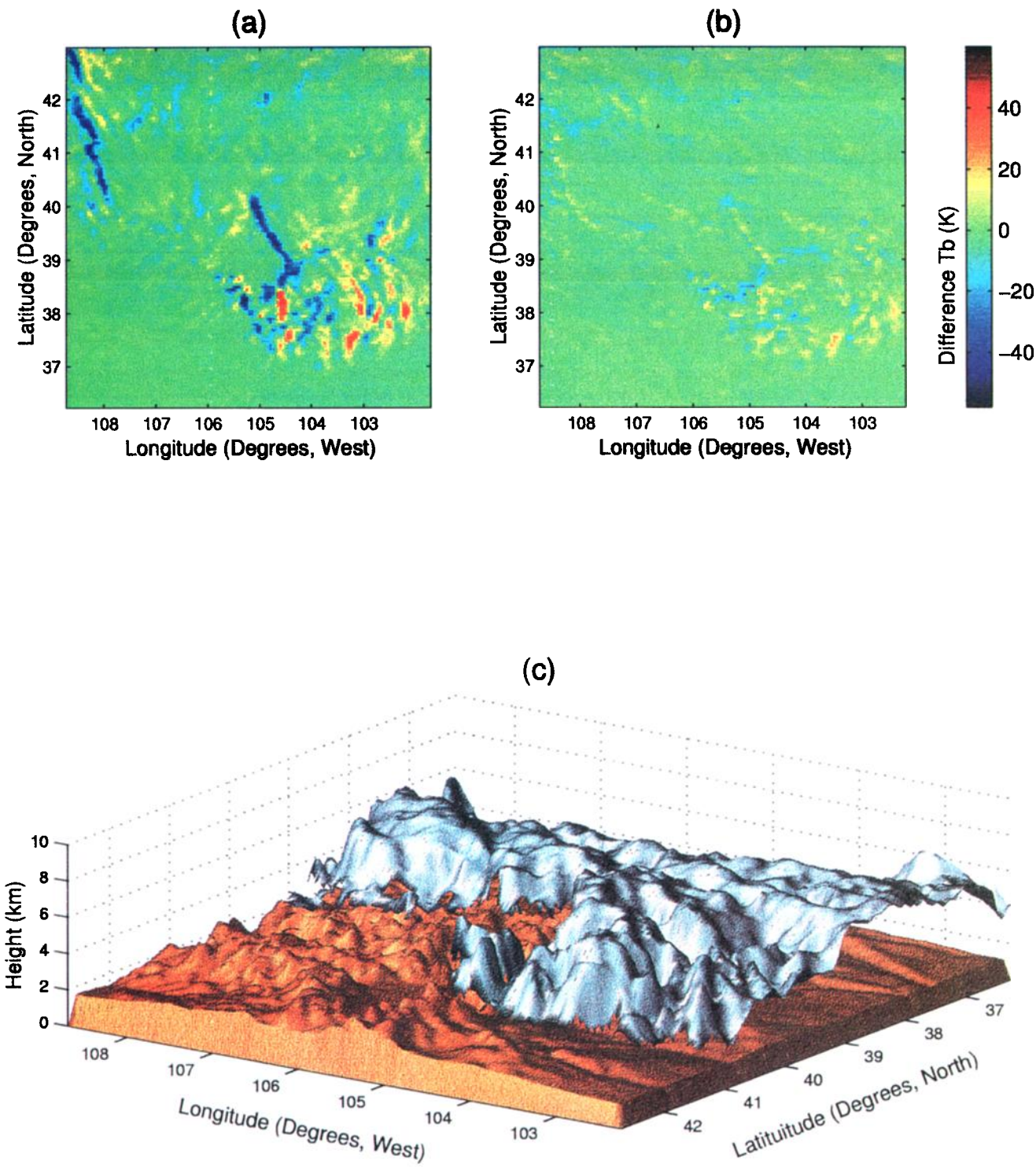

Plate 1. Illustration of the algorithm's products for a single pair of images (pair 9 from Table 1): (a) the image difference between two corresponding original GOES IR images (before adjustment); (b) the image difference between the same corresponding GOES IR images after adjustment; and (c) 3-D cloud top height field superimposed over the shaded relief of the image region.

The method was evaluated with respect to pattern correlation (i.e., the cloud top brightness temperature fields) of the scan-synchronous images before and after the displacement adjustments and by comparing the derived -h relationship with sounding measurements of the atmospheric temperature profiles. With respect to the validity of piecewise linear approximation, the results indicate that with the exception of the lower portion of the troposphere and the troposphere-stratosphere transition zone, the proposed stereoscopic method can approach the atmospheric T_b-h relationship with an accuracy of 0.5km.

The method was used to remap brightness temperature fields from GOES 8 and GOES 9 scan-synchronous pairs over several locations. The remapped images showed substantial improvement in the values of the correlation coefficient as well as in RMSE values. This indicates the method's ability to adequately account for and correct the spatial displacements associated with cloud top heights without the need for massively parallel computers. Clearly, such a technique can be very useful to many researchers who need to generate adequate first-order approximations of cloud height or T_b fields. In summary, the products of the presented algorithm, including cloud image displacements, 3-D cloud top surface, and the atmospheric temperature profile, are expected to be useful for many atmospheric, land surface, and hydrologic studies.

Acknowledgments. This research was supported by NASA grants (NAG5-3460) and (NAG5-7716) and NSF grant (DGE-9355029#3). In addition, the authors wish to thank Kuo-lin Hsu for his useful suggestions and valuable help. We also acknowledge our colleague, Dan Braithwaite, for his assistance in obtaining, archiving, and subsetting the GOES 8 and GOES 9 images used in this study. Last, but not least, we thank Corrie Thies for kindly proofreading this manuscript and for her valuable editorial assistance.

References

Barkstrom, B.R., and G.L. Smith, The Earth Radiation Budget Experiment: Science and implications, *Rev. Geophys., 2*, 379-390, 1986.

Bristor, C.L., and W. Pitchel, 3-D cloud viewing using overlapped pictures from two geostationary satellites, *Bull. Am. Meteorol. Soc., 55*, 1353-1355, 1974.

Cox, S.K., D.S. McDoughal, D.A. Randall, and R.A. Schiffer, FIRE–The first ISCCP regional experiment, *Bull. Am. Meteorol. Soc., 68*, 114-118, 1987.

Duan, Q., S. Sooroshian, and V.K. Gupta, Optimal use of the SCE-UA global optimization method for calibrating watershed models, *J. Hydrol., 158*, 265-284, 1994.

Fujita, T.T., Principles of stereoscopic height computations and their applications to stratospheric cirrus over severe thunderstorms, *J. Meteorol. Soc. Jpn., 60*, 355-368, 1982.

Hasler, A.F., Stereoscopic observations from satellites, An important new tool for the atmospheric sciences, *Bull. Am. Meteorol. Soc., 62*, 194-212, 1981.

Hasler, A.F., and K.R. Morris, Hurricane structure and wind fields from steroscopic and infrared satellite observations and radar data, *J. Clim. Appl. Meteorol. 25*, 709-727, 1986.

Hasler, A.F., R. Mack, and A. Negri, Stereoscopic observations from meteorological satellites, *Adv. Space Res., 2*(6), 105-113, 1983.

Hasler, A.F., J. Strong, R.H. Woodward, and H. Pierce, Automatic-analysis of stereoscopic satellite image pairs for determination of cloud-top height and structure, *J. Appl. Meteorol., 62*, 257-281, 1991.

Kuczera, G., Efficient subspace probabilistic parameter optimization for catchment models, *Water Resour. Res., 33*(1), 177-185, 1997.

Lorenz, D., Stereoscopic imaging from polar orbit and synthetic stereo imaging, *Adv. Space Res.*, 2(6), 133-142, 1983.

Mack, R.A., A.F. Hasler, and R.F. Adler, Thunderstorm cloud-top observations using satellite stereoscopy, *Mon. Weather Rev., 111*, 1949-1964, 1983.

Menzel, W.P. and J.F.W. Purdom, Introducing GOES-I: The first of a new generation of Geostationary Operational Environmental Satellites, *Bull. Am. Meteorol. Soc., 75*, 757-781, 1994.

Minzner, R.A., W.E. Shenk, J. Steranka, and R.D. Teagle, Cloud-top heights determined stereographically from imagery recorded simultaneously by two synchronous meteorological satellites, SM-1 and SMS-2, *Eos Trans. AGU, 57*, 593, 1976.

Nieman, S.J., J. Schmetz, and W.P. Menzel, A comparison of several techniques to assign heights to cloud tracers, *J. Appl. Meteorol., 32*, 1559-1568, 1993.

Rodgers, E., R. Mack, and A.F. Hasler, A satellite steroscopic technique to estimate tropical cyclone intensity, *Mon. Weather. Rev., 111*, 1599-1610, 1983.

Rossow, W.B., Measuring cloud properties from space: A review, *J. Clim., 2*, 201-213, 1989.

Rossow, W.B., and R.A. Schiffer, ISCCP cloud data products, *Bull. Am. Meteorol. Soc., 72*, 2-20, 1991.

Schiffer, R.A., and W.B. Rossow, The International Satellite Cloud Climatology Project (ISCCP): The first project of the World Climate Research Program, *Bull. Am. Meteorol. Soc., 64*, 779-784, 1983.

Sorooshian S., Q.Y. Duan, and H.V. Gupta, Calibration of rainfall runoff models: application of global optimization to the Sacramento soil moisture accounting model, *Water Resour. Res., 29*(4), 1185-1194, 1993.

Sorooshian S., and H. V. Gupta, Model calibration, *in Computer Model of Watershed Hydrology*, Edited by V. Singh, pp. 25-63, Water Resour., Littleton, Colo., 1995.

Strong, J.P., and H.K. Ramapriyan, Massively parallel correlation techniques to determine local differences, paper presented at the Second International Conference on Supercomputing, Int. Supercomput. Inst., Santa Barbara, Calif., 1987.

Thyer, M., G. Kuczera, and B. C. Bates, Probabilistic optimization for conceptual rainfall-runoff models: A comparison of the shuffled complex evolution and simulated annealing algorithms. *Water Resour. Res. 35*(3), 767-773, 1999.

Wylie, D.P., D. Santek, and D.O.C. Starr, Cloud-top height from GOES-8 and GOES-9 stereoscopic imagery, *J. Appl. Meteorol., 37*, 405–413, 1998.

X. Gao, B. Imam, S. E. Mahani, and S. Sorooshian, Department of Hydrology and Water Resources, University of Arizona, Tucson, AZ 85721-0011. (gao@hwr.arizona.edu; bisher@hwr.arizona.edu; mahani@hwr.arizona.edu; soroosh@hwr.arizona.edu.)

(Received July 9, 1999; revised December 9, 1999; accepted December 16, 1999.)